American Mineralogist, Volume 76, pages 83–91, 1991

Crystallographic orientation dependence of mean etchable fission track length in apatite: An empirical model and experimental observations

Raymond A. Donelick
Department of Geology, Rensselaer Polytechnic Institute, Troy, New York 12180-3590, U.S.A.

Abstract

Partially annealed thermal-neutron-induced fission tracks in apatite exhibit mean etchable lengths that range continuously between a maximum for tracks oriented parallel to the crystallographic **c**-axis and a minimum for tracks perpendicular to **c**. A simple empirical model quantifies this crystallographic orientation dependence based on the assumption that the mean etchable fission track length at any angle to the **c**-axis is given by the corresponding radius of an ellipse. The ellipse has semiaxes equal to, respectively, the mean track lengths parallel (l_c) and perpendicular (l_a) to the **c**-axis.

The elliptical model is tested against 61 isothermal partial annealing experiments performed on thermal-neutron-induced fission tracks in Tioga apatite. It is found to adequately characterize etchable fission track length distributions in partially annealed apatites when $l_a \geq 8.4$ μm. The difference between l_c and l_a increases systematically and continuously as both mean lengths decrease, and fission-track lengths are distributed normally about their mean with a standard deviation of ca. 0.75 μm, regardless of crystallographic orientation and relative degree of partial annealing. For $l_a < 8.4$ μm, the elliptical model apparently fails because tracks at relatively high angles to the *c*-axis experience greatly accelerated etchable length reduction.

Experimentally determined values of l_c and l_a in apatite have greater physical significance than does the arithmetic (conventional) mean fission track length. Application of the proposed elliptical annealing model to controlled laboratory experiments may provide valuable insight, heretofore unattainable, into the physical process(es) by which fission tracks anneal in apatite.

Introduction

Charged-particle tracks in various natural and synthetic solid-state nuclear track detectors (SSNTDs) are successfully utilized to study a variety of problems in nuclear physics, chemistry, cosmic-ray physics, geochronology, anthropology, and archaeology, among others. Most charged-particle track applications rely on measured values of track densities (tracks per unit area crossing an etched surface of the SSNTD) and/or etchable track-length distributions. Owing to this, much research has focused on how these two measured quantities depend on the physical properties of the incident particles and the SSNTD (e.g., Fleischer et al., 1964; Dartyge et al., 1981; Albrecht et al., 1985; Carlson, 1990) and the environmental conditions experienced by the tracks (e.g., Fleischer et al., 1965; Naeser and Faul, 1969; Green et al., 1986; Donelick et al., 1990).

Fission tracks in apatite, a special case of charged-particle tracks, record detailed time-temperature information experienced by rocks located within the upper several kilometers of the Earth's crust. This property is a direct consequence of (1) the continual production of new fission track populations in apatite through geological time and (2) a measurable decrease in the integrated thermal history recorded by progressively younger track populations (Green et al., 1989; Donelick and Willett, 1989; Corrigan and Wilson, 1989). Apatite fission-track data serve to constrain geodynamical models of orogenesis (e.g., Wagner et al., 1977; Zeitler, 1983), subduction (e.g., Dumitru, 1989), continental rifting (e.g., Kelley and Duncan, 1986), and sedimentary basin evolution (e.g., Naeser, 1979; Gleadow and Duddy, 1981).

Many workers have studied the thermal stability of fission tracks in apatite, utilizing variations in (1) track densities (e.g., Naeser and Faul, 1969), (2) external or projected etchable track-length distributions (e.g., Dakowski, 1978; Wagner, 1981) or (3) internal or confined etchable track-length distributions (e.g., Bhandari et al., 1971; Green and Durrani, 1977; Green et al., 1986; Donelick et al., 1990; Crowley et al., in preparation). Etchable length distributions of confined fission tracks provide a more fundamental measure of the relative degree of track annealing and can be measured with greater precision than either track densities or projected track length distributions (Laslett et al., 1982).

Green and Durrani (1977) first observed that the mean

* Present address: Department of Geology and Geophysics, Rice University, Houston, Texas 77251, U.S.A.

0003–004X/91/0102–0083$02.00

Table 1. Summary of the chemical composition data (wt%) obtained by electron microprobe analysis for Tioga and Durango apatite

Apatite	Tioga (all)	Tioga (core)	Tioga (rim)	Durango
Number of analyses	16	8	8	20
P_2O_5	40.98(23)	41.06(28)	40.92(18)	40.18(20)
CaO	53.27(28)	53.21(25)	53.32(31)	53.82(29)
F	2.35(16)	2.37(10)	2.34(21)	3.32(22)
Cl	0.54(02)	0.53(02)	0.54(02)	0.35(01)
SrO	0.03(02)	0.03(02)	0.04(01)	0.06(01)
FeO	0.85(09)	0.84(08)	0.85(10)	0.05(03)
MnO	0.42(05)	0.42(06)	0.41(04)	n.d.
SiO_2	0.03(04)	0.04(04)	0.03(04)	0.33(01)
Na_2O	0.17(02)	0.17(02)	0.17(01)	0.25(02)
Ce_2O_3	0.17(03)	0.18(02)	0.16(04)	0.72(03)
As_2O_5	n.d.	n.d.	n.d.	0.01(01)
Total	98.81	98.85	98.78	99.09

Note: Numbers in parentheses are 1 standard deviation (in significant figures) for the respective values; n.d. = none detected.

etchable length of a single population of fission tracks in apatite varies with crystallographic orientation. Tracks oriented parallel to the c-axis exhibit a greater mean etchable length than tracks perpendicular to c, especially at relatively high degrees of partial annealing. Several later investigations supported this finding (Green, 1981; Green et al., 1986; Donelick et al., 1990; Crowley et al., in preparation). The purpose of this study is twofold: (1) to present an empirical model, based on the crystal symmetry of apatite, that quantifies the dependence of mean etchable fission track length in apatite on track orientation and (2) to test this model against a series of isothermal partial annealing experiments.

Experimental procedures

Sample details

The apatite chosen for this study was obtained from an outcrop of the 390 Ma Tioga ash bed (bed B; Way et al., 1986) located near Old Port, Pennsylvania, U.S.A. (Roden et al., 1990; John H. Way, personal communication, 1987). Several grams of euhedral (typical mean diameter ca. 150 μm), chemically homogeneous Tioga apatite grains (Table 1) were recovered using standard heavy liquid and magnetic mineral separation techniques. Interestingly, some of the apatite grains possess external surfaces that have been naturally etched, probably by humic acids, revealing faint fission tracks.

Annealing experiments

The Tioga apatite was heated in air at 1 atm for 12 h at 500 °C to completely anneal all natural fission tracks. Only one natural confined fission track was observed to have survived this heat treatment, presumably because it was naturally etched, in more than 1000 annealed Tioga apatite grains prepared as a control. Several grams of the annealed apatite were irradiated with thermal neutrons at the Oregon State University TRIGA reactor in Corvallis (fluence = 8×10^{15} neutrons/cm^2) to induce the fission of ^{235}U nuclei and form fresh fission tracks. Forty mg aliquot parts of the irradiated apatite were heated in a tube furnace at 1 atm to partially anneal the induced fission tracks for times ranging from about 18 min to 3 weeks at temperatures ranging from 195 to 407 °C (temperature fluctuations during heat treatment estimated to be ± 1–3 °C as indicated in Table 2). Two additional 40 mg aliquot parts of the irradiated apatite were heated in a drying oven at 1 atm and 100 °C for approximately 94 and 242 d respectively.

Standard mounting and polishing procedures were employed for all experiments. The polished surfaces of a majority of grains in each mount represented crystallographic planes parallel to the c-axis owing to the prismatic habit of the Tioga apatite. All polished mounts were etched for 25 s at 21 °C in 5 N HNO_3. Immediately after etching, each sample was washed first in H_2O, then in ethanol, and heated for 10 min at 150 °C on a hot plate. This washing and drying procedure served to remove any residual fluid trapped in the etched tracks.

Track length and orientation measurement

Only horizontal, confined fission tracks lying in crystallographic planes parallel to the c-axis were measured in this study (Fig. 1). The following criteria were used to identify appropriately oriented Tioga apatite grains in unpolarized transmitted and reflected light (e.g., Donelick, 1988): (1) the presence of a linear interface between the grain and the epoxy where an inclined prismatic face is intersected by the polished surface and (2) elongate etch pit cross-sections that are aligned parallel to the c-axis due to bulk etching anisotropy (e.g., Singh et al., 1986). Tracks were viewed in unpolarized transmitted light at 1562.5× (12.5× oculars, 1.25× projection tube, 100× dry objective). Individual track lengths and angles to c were measured using a digitizing tablet interfaced with a personal computer for rapid data retrieval and subsequent manipulation. Positioning of the cursor (with an attached LED point source) on the digitizing surface was made possible by a projection tube affixed to the microscope. The digitizing surface was calibrated for length measurement using a diffraction grating with 600 lines/mm. The length of each track and its angle to the c-axis were computed from three digitized points (Fig. 1b), one at each end of the track and a third along the c-axis from the second. Repeated measurements performed on individual fission tracks indicate that the measurement precisions (1 standard deviation) of individual lengths and angles are ca. 0.15 μm and ca. 2° respectively.

Experimental results

Qualitative description

A minimum of 200 (where possible) confined fission track lengths and corresponding track angles to the crystallographic c-axis were measured for the 61 partial annealing experiments performed in this study (Table 2). Green and Durrani (1977), among others, demonstrated

TABLE 2. Summary of the experimental results

Experiment	ln(*t*) (*t* in s)	*T* °C	*N*	θ_m (deg)	l_m (μm)	l_c (μm)	l_a (μm)	σ_m (μm)	σ_e (μm)	χ^2	ν	*Q*
TI026*	5.886	23(2)	155	51.8(16)	17.08(07)	17.50(14)	16.80(10)	0.89	0.87	205.1	153	0.003
TI027*	6.492	23(2)	118	55.2(20)	17.06(08)	17.43(17)	16.86(11)	0.91	0.90	167.7	116	0.001
TI024*	6.802	23(2)	130	55.8(18)	16.91(07)	17.20(17)	16.76(10)	0.74	0.73	122.7	128	0.616
TI025*	6.928	23(2)	178	54.2(17)	17.06(06)	17.38(13)	16.87(09)	0.83	0.82	210.5	176	0.039
TI028*	14.427	23(2)	139	53.3(18)	16.77(08)	17.31(15)	16.45(10)	0.91	0.87	187.1	137	0.003
TI023*	15.833	23(2)	220	53.6(14)	16.58(06)	17.10(12)	16.28(08)	0.84	0.81	253.1	218	0.052
TI022*	16.195	23(2)	220	53.8(13)	16.66(05)	17.16(13)	16.37(08)	0.79	0.76	225.9	218	0.342
TI021	15.915	100(3)	220	51.5(16)	16.12(06)	16.59(11)	15.81(08)	0.83	0.79	242.8	218	0.120
TI033	16.858	100(3)	264	52.7(12)	15.63(05)	16.24(11)	15.27(07)	0.86	0.81	308.1	262	0.027
TI011	11.498	195(3)	215	50.7(14)	15.18(05)	15.76(12)	14.79(08)	0.78	0.72	195.8	213	0.795
TI006	12.000	195(3)	217	51.8(14)	15.14(06)	15.65(12)	14.81(08)	0.87	0.83	266.7	215	0.009
TI012	12.500	195(3)	218	51.0(13)	15.05(05)	15.88(13)	14.51(08)	0.76	0.66	167.5	216	0.994
TI013	13.000	195(3)	219	53.8(14)	14.98(05)	15.53(13)	14.67(08)	0.77	0.73	204.6	217	0.717
TI014	13.500	195(3)	211	52.4(13)	14.82(06)	15.62(13)	14.36(08)	0.83	0.75	208.6	209	0.494
TI015A**	14.000	195(3)	216	52.3(14)	14.73(05)	15.45(13)	14.31(08)	0.77	0.69	183.8	214	0.933
TI015B**	14.000	195(3)	230	53.0(13)	14.70(05)	15.56(13)	14.21(08)	0.79	0.70	197.1	228	0.931
TI008	14.501	195(3)	222	51.5(13)	14.63(05)	15.35(12)	14.19(08)	0.75	0.67	173.9	220	0.990
TI004	11.000	290(3)	201	51.1(15)	12.99(06)	13.81(12)	12.47(08)	0.86	0.76	204.7	199	0.376
TI016	11.501	290(3)	208	50.8(15)	12.80(06)	13.83(12)	12.17(08)	0.87	0.70	180.7	206	0.898
TI005	12.000	290(3)	215	51.5(15)	12.51(06)	13.44(12)	11.94(08)	0.92	0.81	248.5	213	0.048
TI017	12.500	290(3)	237	50.6(14)	12.26(06)	13.61(12)	11.42(08)	0.99	0.73	226.6	235	0.642
TI018	13.000	290(3)	216	54.5(13)	11.68(06)	12.98(15)	11.06(08)	0.91	0.74	211.4	214	0.538
TI019	13.500	290(3)	211	52.1(14)	10.97(07)	12.44(14)	10.18(08)	0.96	0.73	198.2	209	0.692
TI020A**	14.000	290(3)	218	49.3(14)	10.66(07)	12.46(14)	9.58(08)	1.08	0.71	194.4	216	0.852
TI020B**	14.000	290(3)	220	48.5(14)	10.58(08)	12.18(13)	9.55(08)	1.11	0.80	249.3	218	0.071
TI007	14.501	290(3)	214	46.3(13)	10.10(07)	11.70(13)	8.85(08)	1.07	0.72	197.0	212	0.762
TI035	7.090	247(1)	249	51.5(13)	14.98(05)	15.73(12)	14.50(08)	0.85	0.77	259.9	247	0.274
TI039	7.090	258(1)	228	49.6(14)	14.99(05)	15.54(11)	14.59(08)	0.72	0.66	177.5	226	0.993
TI043	7.090	269(1)	230	49.5(15)	14.97(06)	15.79(11)	14.38(08)	0.85	0.73	214.4	228	0.731
TI046	7.090	279(1)	253	52.2(14)	14.76(05)	15.71(11)	14.18(07)	0.86	0.72	230.0	251	0.826
TI049	7.090	290(1)	283	54.9(12)	14.77(05)	15.56(12)	14.37(07)	0.82	0.75	282.7	281	0.460
TI052	7.090	302(1)	267	53.9(13)	14.21(05)	15.09(11)	13.71(07)	0.88	0.77	280.7	265	0.243
TI041	7.090	311(1)	245	51.0(13)	14.18(05)	14.99(11)	13.66(08)	0.78	0.68	198.8	243	0.982
TI042	7.090	323(1)	241	50.8(15)	13.83(06)	14.83(11)	13.19(07)	0.90	0.74	230.8	239	0.636
TI045	7.090	332(1)	254	52.4(13)	13.47(05)	14.44(12)	12.89(07)	0.83	0.70	217.9	252	0.941
TI048	7.090	342(1)	284	55.2(12)	12.91(05)	14.09(12)	12.34(07)	0.89	0.75	281.3	282	0.500
TI051	7.090	351(1)	272	54.3(13)	12.19(06)	13.49(12)	11.54(07)	0.91	0.73	256.2	270	0.718
TI054	7.090	357(1)	256	52.5(13)	11.93(07)	13.52(13)	11.09(07)	1.05	0.80	289.1	254	0.064
TI055	7.090	366(1)	275	54.3(13)	11.88(06)	13.23(12)	11.20(07)	0.99	0.78	299.3	273	0.131
TI053	7.090	373(1)	252	52.6(14)	11.56(06)	13.04(12)	10.74(07)	1.03	0.76	254.6	250	0.408
TI050	7.090	380(1)	254	52.3(13)	11.13(06)	12.78(13)	10.25(07)	1.01	0.71	224.0	252	0.897
TI047	7.090	387(1)	231	40.3(13)	9.88(08)	11.49(11)	8.35(08)	1.18	0.74	224.2	229	0.577
TI044	7.090	394(1)	217	41.8(14)	9.98(09)	11.62(12)	8.54(08)	1.26	0.88	300.4	215	0.000
TI040	7.090	400(1)	239	39.4(16)	7.38(18)	11.35(13)	4.84(06)	2.76	1.53	995.1	237	0.000
TI038†	7.090	407(1)	—	—	—	—	—	—	—	—	—	—
TI030	11.000	200(1)	240	50.5(14)	15.03(05)	15.66(11)	14.62(08)	0.83	0.77	253.0	238	0.241
TI034	11.008	211(1)	272	54.2(13)	15.06(05)	15.72(11)	14.70(07)	0.80	0.74	264.3	270	0.587
TI036	11.002	221(1)	264	53.3(13)	14.88(05)	15.54(11)	14.49(07)	0.84	0.78	283.5	262	0.172
TI056	11.000	231(1)	281	54.8(12)	14.69(04)	15.34(12)	14.35(07)	0.75	0.69	239.4	279	0.959
TI059	11.012	241(1)	231	49.4(14)	14.50(06)	15.29(11)	13.93(08)	0.84	0.73	217.0	229	0.706
TI062	11.000	250(1)	253	52.2(13)	14.39(05)	15.19(12)	13.91(08)	0.79	0.69	216.3	251	0.945
TI065	11.000	259(1)	244	51.1(14)	14.13(05)	14.86(11)	13.66(08)	0.79	0.70	213.4	242	0.907
TI067	11.000	270(1)	273	54.3(13)	13.87(05)	14.91(11)	13.33(07)	0.88	0.74	266.0	271	0.575
TI066	11.000	280(1)	251	52.2(13)	13.46(05)	14.43(12)	12.89(08)	0.85	0.73	237.4	249	0.690
TI063	11.000	290(1)	273	54.2(13)	13.01(06)	14.17(12)	12.40(07)	0.91	0.75	273.0	271	0.455
TI057	11.000	302(1)	278	54.3(12)	12.51(05)	13.82(12)	11.87(07)	0.91	0.73	263.5	276	0.696
TI060	11.010	308(1)	270	54.0(13)	11.79(06)	12.92(12)	11.21(07)	0.93	0.80	304.7	268	0.061
TI037	11.000	315(1)	263	53.3(12)	11.16(06)	12.74(13)	10.37(07)	0.97	0.73	245.5	261	0.747
TI058	11.000	323(1)	277	53.7(12)	11.16(06)	12.88(13)	10.32(07)	1.01	0.71	247.6	275	0.881
TI031	11.000	328(1)	203	45.3(14)	10.04(08)	11.78(13)	8.77(08)	1.14	0.75	202.1	201	0.464
TI068	11.000	333(1)	209	46.3(15)	10.13(08)	11.84(12)	8.92(08)	1.18	0.77	221.5	207	0.233
TI061	11.008	339(1)	216	42.7(14)	9.84(08)	11.61(12)	8.40(08)	1.21	0.78	231.0	214	0.202
TI064†	11.000	347(1)	—	—	—	—	—	—	—	—	—	—

Note: Numbers in parentheses are 1 standard deviation (in significant figures) for the respective values.
* Recalculated from Donelick et al. (1990).
** Labels A and B indicate duplicate analyses of the same sample mount.
† Experiments with too few tracks to permit measurement.

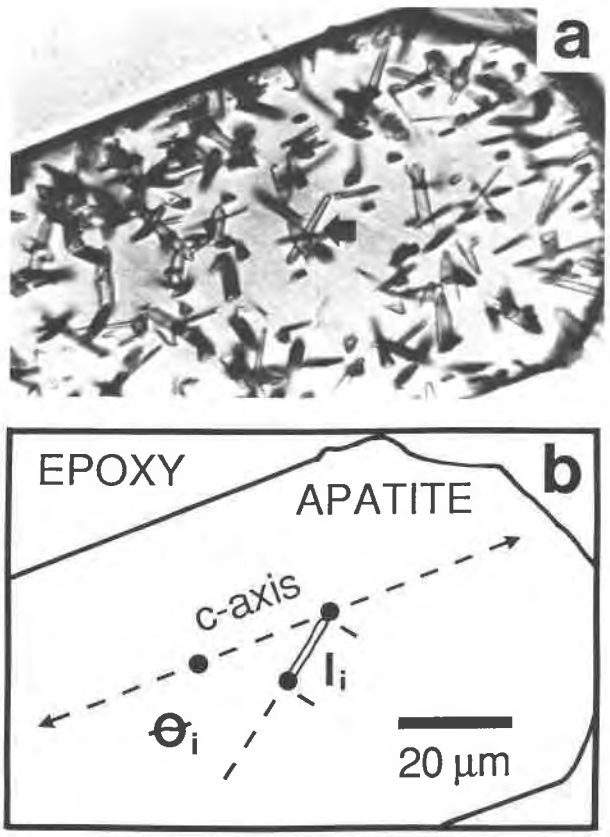

Fig. 1. (**a**) Photomicrograph of a horizontal confined fission track, indicated by the arrow, in Tioga apatite. (**b**) Schematic representation of **a** with the crystallographic **c**-axis indicated and the three points, indicated by solid dots, used for track length (l_i) and orientation (θ_i) measurement.

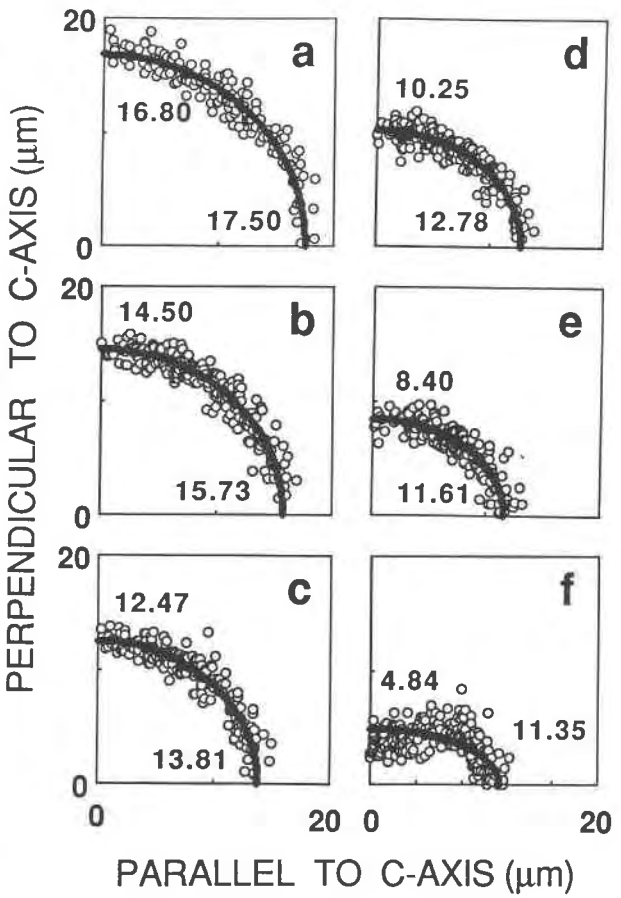

Fig. 2. Polar coordinate plots of six fission track length populations spanning the range of annealing conditions studied. Best-fit ellipses are drawn in as solid curves and the lengths of their respective semiaxes are labeled (uncertainties given in Table 2). (**a**) TI026 annealed 6 min at 23 °C, (**b**) TI035 annealed 20 min at 247 °C, (**c**) TI004 annealed 16 h 38 min at 290 °C, (**d**) TI050 annealed 20 min at 380 °C, (**e**) TI061 annealed 16 h 46 min at 339 °C, and (**f**) TI040 annealed 20 min at 400 °C.

that the mean etchable fission track length in partially annealed apatite varies continuously between a maximum for tracks oriented parallel to the crystallographic **c**-axis and a minimum for tracks perpendicular to **c**. All published graphical representations of this effect depict track length vs. track angle to the **c**-axis in Cartesian coordinates (Green and Durrani, 1977; Laslett et al., 1982; Green et al., 1986). A more physically meaningful representation is to plot these same values in polar coordinates. This is done in Figure 2 for six partially annealed fission track populations in Tioga apatite, arranged in order of increasing degree of annealing (i.e., decreasing arithmetic mean track length).

Apatite belongs to the centrosymmetrical class $6/m$ of the hexagonal crystal system. The empirical model adopted in this study is based on the assumption that fission tracks in apatite, lying within crystallographic planes parallel to the **c**-axis, exhibit etchable lengths that are distributed about an ellipse. The ellipse has semiaxes equal to the mean track lengths parallel and perpendicular to **c**. Rotation of the ellipse about the **c**-axis creates a triaxial ellipsoid with radii that correspond to the mean etchable fission track lengths in all crystallographic directions. The mean fission-track length ellipsoid is analogous to the more familiar uniaxial optical indicatrix. For each of the track length populations in Figure 2, best-fit ellipses are drawn in as solid curves. The track lengths for the first five cases in Figure 2 (Figs. 2a–2e) appear to be evenly distributed about the first quadrant of their respective ellipse. A notable exception to this apparent behavior is observed for the most severely annealed case in Figure 2f. In this case, the individual track lengths oriented at angles greater than approximately 25° to the crystallographic **c**-axis exhibit a significant departure from their best-fit ellipse.

Quantitative description

Mean etchable fission track lengths. Green et al. (1986) investigated the variation between the arithmetic mean track length and partial annealing conditions. Table 2 presents the arithmetic mean track lengths (l_m), including

error estimates (significant figures in parentheses), and the arithmetic mean track angles to the crystallographic c-axis (θ_m) calculated for the 61 partial annealing experiments performed in this study. The notation used here and below is summarized in Appendix 1.

Best-fit ellipses, like those depicted in Figure 2, are calculated for each set of track lengths as follows. Consider an ellipse with semiaxes l_c and l_a. The polar coordinate equation for the radius of this ellipse at an angle θ_i to semiaxis l_c is (after Beyer, 1987)

$$l_{\theta_i} = \left\{ \frac{\sin^2\theta_i}{l_a^2} + \frac{\cos^2\theta_i}{l_c^2} \right\}^{-1/2}. \quad (1)$$

In the elliptical annealing model, l_c and l_a are the mean track lengths parallel and perpendicular to the crystallographic c-axis, respectively, and l_{θ_i} equals the mean length at an angle θ_i to c. Equation 1 is equivalent to the function $E[l/\theta]$ used by Galbraith and Laslett (1988, p. 308) to formulate mean etchable fission track length in apatite and relate this mean to track density. The best-fit values of l_c and l_a for a set of N confined track lengths (l_i) and corresponding track angles to the c-axis (θ_i) are those for which the chi-square statistic (χ^2), calculated as follows, is minimized (after Press et al., 1986, p. 502–504; Donelick, 1988).

$$\chi^2 = \sum_{i=1}^{N} \left(\frac{l_i - l_{\theta_i}}{\sigma_{\theta_i}} \right)^2 \quad (2)$$

The value of l_{θ_i} is calculated from Equation 1. The parameter σ_{θ_i} represents the standard deviation of track lengths about the radius of the ellipse at an angle θ_i to the c-axis and is derived below. Calculated values of l_c and l_a for each partial annealing experiment are tabulated in Table 2, with their estimated errors (see below) given in parentheses.

Fission track length distributions. The conventional distribution is defined here as the distribution of track lengths about their arithmetic mean and the elliptical distribution is defined as the distribution of track lengths about their best-fit ellipse. The elliptical distribution analysis includes, as a special case, the conventional approach. For track lengths measured in crystallographic planes parallel to the c-axis, the conventional approach is equivalent to calculating the distribution of track lengths about their best-fit circle, the radius of which equals the arithmetic mean track length (replace l_{θ_i} in Eq. 2 with l_m, the arithmetic mean length). The standard deviation of the conventional track-length distribution (σ_m) is routinely calculated and reported. The more general approach is to permit the mean track length to vary with track angle to the crystallographic c-axis by replacing l_m in the conventional distribution analysis with l_{θ_i}, given by Equation 1. This leads to the following expression for the standard deviation (σ_e) of the distribution of track lengths about their best-fit ellipse.

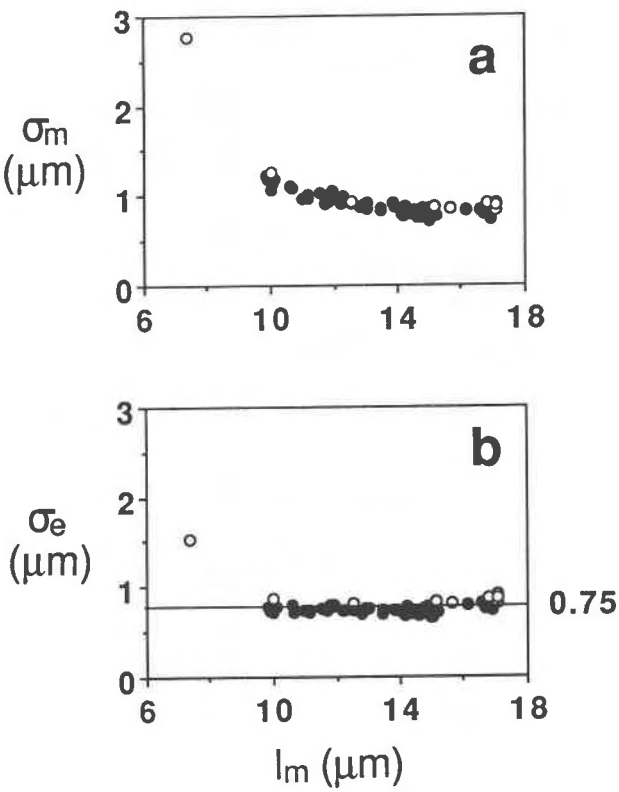

Fig. 3. (a) Conventional standard deviation (σ_m) vs. arithmetic mean fission track length (l_m). (b) Elliptical standard deviation (σ_e) vs. arithmetic mean fission track length (l_m). Typical 2σ error bar for l_m is approximately as wide as the symbols used. Solid symbols, $Q \geq 0.05$; open symbols, $Q < 0.05$.

$$\sigma_e = \left\{ \frac{1}{N-1} \sum_{i=1}^{N} (l_i - l_{\theta_i})^2 \right\}^{1/2} \quad (3)$$

The calculated values of σ_m and σ_e for this study are given in Table 2 and are plotted against the arithmetic mean length (l_m) in Figure 3. Two significant trends are apparent in these data. First, σ_e is less than σ_m in all cases, an expected result because of the greater number of fitted parameters in the elliptical analysis vs. the conventional analysis. Second, σ_e is constant at ca. 0.75 μm over virtually the full range of l_m encountered, with the notable exception of sample TI040 (e.g., Fig. 2f). The value of σ_m, however, increases systematically and continuously as l_m decreases, an observation first reported by Green et al. (1986).

Expressions similar to Equation 3 can be written for the skewness and excess kurtosis of the elliptical distribution (Donelick, 1988). Although not reported, the latter parameters are found to fluctuate randomly about zero indicating that fission track lengths are distributed approximately normally about their best-fit ellipses.

Estimated goodness of fit of the elliptical annealing model. The value of χ^2 may be calculated from Equation 2 once the parameter σ_{θ_i}, a measure of the width of the

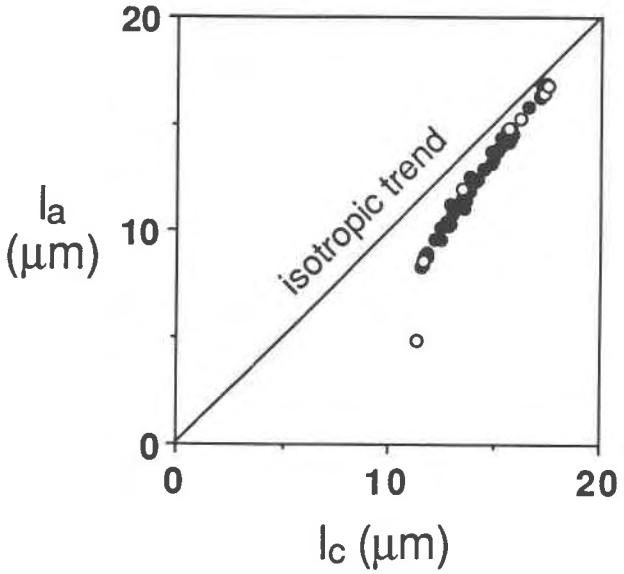

Fig. 4. Mean fission track length parallel (l_c) vs. mean length perpendicular (l_a) to the crystallographic c-axis. Typical 2σ error boxes are approximately the same size as the symbols used. The trend for isotropic etchable fission track-length reduction is along the straight line. Solid circles, $Q \geq 0.05$; open circles, $Q < 0.05$.

distribution of track lengths about the ellipse at an angle θ_i to the c-axis, is known (see Press et al., 1986, p. 503). The parameter σ_{θ_i} is not known a priori but Figures 2a–2e imply it is constant over all orientations and degrees of annealing, with the notable exception of the most severely annealed case (Fig. 2f). The elliptical standard deviation (σ_e) is simply an average, over all orientations, of the parameter σ_{θ_i}. Because of this, the near constancy of σ_e at 0.75 μm (Table 2 and Fig. 3b) implies that the parameter σ_{θ_i} is independent of the degree of track annealing, except for the most severely annealed cases (e.g., TI040). Therefore, a constant value of 0.75 μm is used

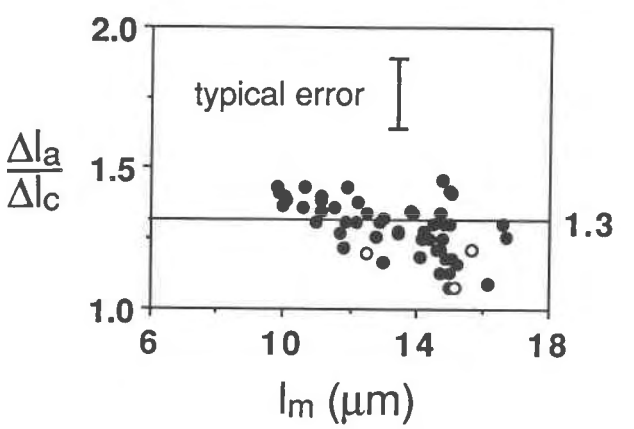

Fig. 5. $\Delta l_a/\Delta l_c$ vs. arithmetic mean fission track length (l_m). A typical 2σ error bar is included. The initial condition used is experiment TI026. Solid circles, $Q \geq 0.05$; open circles, $Q < 0.05$.

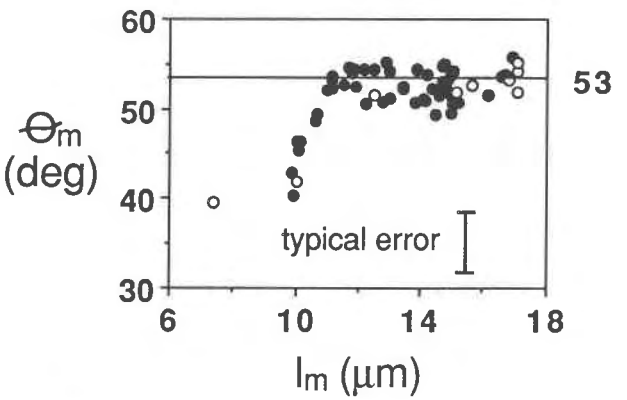

Fig. 6. Arithmetic mean track angle to the crystallographic c-axis (θ_m) vs. arithmetic mean fission track length (l_m). A typical 2σ error bar is included. Solid circles, $Q \geq 0.05$; open circles, $Q < 0.05$.

for the parameter σ_{θ_i} to calculate χ^2 from Equation 2. The number of degrees of freedom (ν) is given by $N - 2$, where 2 corresponds to the number of parameters being fit. The goodness of fit (Q; probability of greater chi-square) is estimated for χ^2 and ν using the incomplete gamma function (Press et al., 1986, p. 160–165). Values of χ^2, ν, and Q calculated for each partial annealing experiment are given in Table 2. The fit is considered good when Q is 0.05 or larger.

Estimated errors of the mean track lengths parallel and perpendicular to the c-axis. Fission track lengths are approximately normally distributed about their best-fit ellipse (Donelick, 1988). Therefore, the square-roots of the diagonal elements in the formal covariance matrix of the fit are valid estimators (1 standard deviation) of the errors of the respective fitted parameters l_c and l_a (Press et al., 1986, p. 534–537).

Discussion

Fifty-two of the 61 measurements passed the chi-square test at the 0.95 confidence level ($Q \geq 0.05$; Table 2). The failures include sample TI040 (Fig. 2f) which, as discussed above, exhibits a significant departure of individual track lengths from its best-fit ellipse at track orientations greater than approximately 25° to the crystallographic c-axis. This particular failure provides statistical evidence that best-fit ellipses do not account for all of the variation in mean fission track length with crystallographic orientation at the highest degrees of track annealing (i.e., l_a less than approximately 8.4 μm). The eight other cases where Q is less than 0.05 are not considered significant insofar as they do not indicate failure of the elliptical annealing model. For all of these cases, other experiments with Q greater than 0.05 were encountered that exhibit similar mean track lengths (for example compare TI027 and TI025 in Table 2).

Experiments TI015 and TI020 were analyzed twice to test the reproducibility of the three mean fission track length types tabulated in Table 2 (l_m, l_c, and l_a). The repeat measurements were performed several months after the

first and the samples were selected randomly and masked by a co-worker to avoid measurement bias. For both samples, the three mean track lengths are reproduced within a limit of two standard deviations (a precision of ca. 2%).

Consider the mean etchable fission track lengths parallel (l_c) and perpendicular (l_a) to the crystallographic c-axis in Table 2. For l_a greater than approximately 8.4 μm (the lower limit of strict applicability of the elliptical annealing model), the following generalizations can be made. First, l_c is greater than l_a in all cases (Fig. 4), the difference increasing systematically and continuously as the degree of partial track annealing increases. This relation holds even for the lowest degrees of track annealing (e.g., experiment TI026), an observation that may be related to the track etching procedures employed (Crowley et al., in preparation; K. Crowley, personal communication, 1990). Second, the ratio $\Delta l_a/\Delta l_c$ is approximately constant at 1.3 (Fig. 5). This feature was first pointed out by Carlson (1990).

Figure 6 is a plot of arithmetic mean track angle to the crystallographic c-axis (θ_m) vs. arithmetic mean track length (l_m) for each experiment. There is an overall decrease of θ_m as l_m decreases, consistent with the increased likelihood of etching tracks at low angles to the crystallographic c-axis as track length anisotropy increases (Laslett et al., 1982). In detail, however, the trend is discontinuous, with θ_m being nearly constant at ca. 53° for l_m greater than ca. 11 μm. The significance of this discontinuous trend is unclear.

The elliptical annealing model is useful for interpreting results obtained from partial annealing experiments because calculated values of l_c and l_a are independent of mean track orientation (θ_m) and they are determined at fixed crystallographic orientation. Consider experiment TI061, which exhibits a strong dependence of mean fission track length on crystallographic orientation (Fig. 2e and Table 2). The lack of dependence of l_c and l_a on θ_m is illustrated in Figure 7 using six different subsets of the 216 track lengths measured for TI061. These six track length subsets are characterized by unique values of θ_m, ranging 60.2° to 27.8°, and include the following tracks (Table 3): (a) only tracks oriented >45° to the crystallographic c-axis; (b) every third track <45° plus all tracks >45°; (c) two of every three tracks <45° plus all tracks >45°; (d) every track <45° plus two of every three tracks >45°; (e) every track <45° plus every third track >45°; and (f) only tracks <45°. The calculated values of l_a and l_c for these six track-length subsets of TI061 are reproducible, within the estimated errors, over the full range of θ_m investigated (Table 3). However, the arithmetic (conventional) mean track length (l_m; Table 3) is not reproducible over the range of θ_m studied.

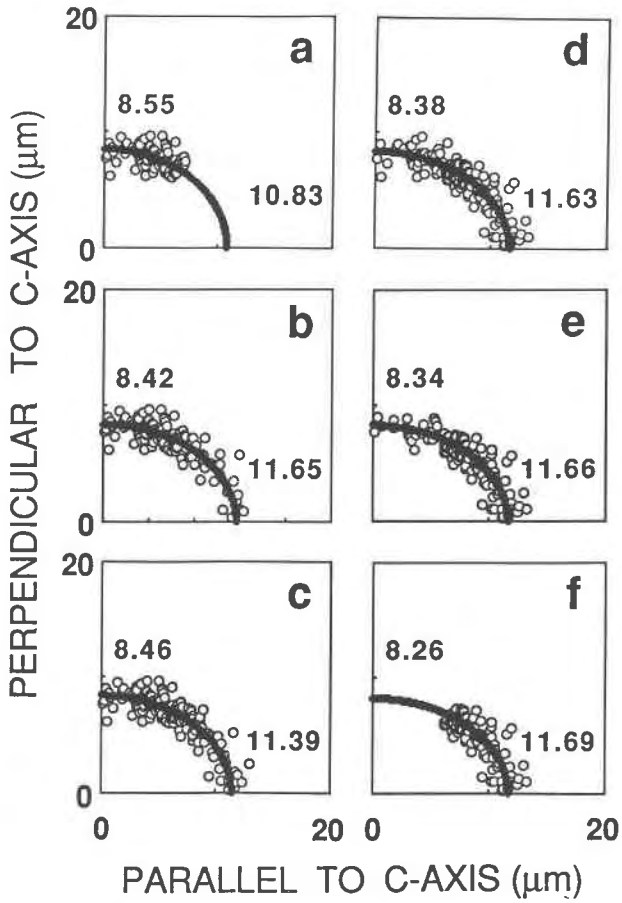

Fig. 7. Polar coordinate plots of six component fission track populations of experiment TI061 (see text; compare to Fig. 2e). Best-fit ellipses are drawn in as solid curves and the lengths of their respective semiaxes are labeled (uncertainties given in Table 3). Values of the arithmetic mean track angle to the crystallographic c-axis (θ_m) for each plot are (a) 60.2°, (b) 51.2°, (c) 48.3°, (d) 37.4°, (e) 35.1°, and (f) 27.8° respectively.

TABLE 3. Summary of the conventional and elliptical distribution analyses for six component fission track populations of experiment TI061

Subset*	N	θ_m (deg)	l_m (μm)	l_c (μm)	l_a (μm)	σ_m (μm)	σ_e (μm)	χ^2	ν	Q
a	99	60.2(12)	9.04(08)	10.83(62)	8.55(14)	0.82	0.77	103.2	97	0.314
b	138	51.2(16)	9.47(10)	11.65(20)	8.42(09)	1.14	0.80	154.3	136	0.135
c	157	48.3(16)	9.56(09)	11.39(16)	8.46(09)	1.12	0.78	168.2	155	0.222
d	166	37.4(15)	10.09(09)	11.63(13)	8.38(10)	1.21	0.80	185.5	164	0.120
e	150	35.1(15)	10.20(10)	11.66(13)	8.34(12)	1.17	0.76	151.4	148	0.408
f	117	27.8(12)	10.52(10)	11.69(14)	8.26(17)	1.05	0.78	125.8	115	0.231

Note: Numbers in parentheses are 1 standard deviation (in significant figures) for the respective values.
* Track length subsets correspond to the plots in Figure 7.

Table 4. Empirical constants for Carlson's (1990) apatite fission-track annealing model

Length type	Applicable range (μm)	n	E_a (kJ mol^{-1})	A (μm)
l_c	11.61–17.20	0.133	206	3.95
l_a	8.40–16.76	0.134	210	6.14

Note: Values were determined by chi-square minimization using values of l_c and l_a from Table 2 for which $Q \geq 0.05$.

The elliptical annealing model may lead to a better understanding of the kinetics of the fission track annealing process as a function of crystallographic orientation. Carlson (1990) quantified a physical model for apatite fission-track annealing that includes three experimentally derived empirical constants: n, related to the defect density distribution in the latent (unetched) fission track; E_a (defined as Q by Carlson, 1990), the activation energy for defect elimination; A, a rate constant. These three empirical constants, determined by chi-square minimization using Carlson's Equation 5 for isothermal heating histories, are compiled in Table 4 for values of l_c and l_a from Table 2 for which $Q \geq 0.05$. Note that the defect-density distribution terms and activation energies for both of these crystallographic orientations are approximately equal. The invariance of the activation energy was first suggested by Donelick (1988) and Ravenhurst et al. (1989).

Conclusions

The proposed elliptical annealing model permits the mean fission track lengths parallel (l_c) and perpendicular (l_a) to the c-axis to be reliably determined, as long as $l_a \geq 8.4$ μm. For $l_a < 8.4$ μm, fission track length distributions are not adequately described by ellipses. The following trends are observed for $l_a \geq 8.4$ μm: (1) calculated values of l_c are always greater than l_a, the difference increasing systematically and continuously as the degree of track annealing increases; (2) $\Delta l_a/\Delta l_c$ is approximately constant at 1.3; and (3) l_c and l_a are independent, within error, of the arithmetic mean track angle to the c-axis.

The etchable lengths of a single population of fission tracks in apatite are distributed normally about their best-fit ellipse with a typical standard deviation of 0.75 μm, as long as $l_a \geq 8.4$ μm. For $l_a < 8.4$ μm, fission tracks at relatively high angles to the c-axis experience accelerated etchable length reduction and the elliptical model fails.

Acknowledgments

The author gratefully acknowledges the financial assistance for this project from a grant to D. Miller by Texaco, Inc. E. Watson generously made available the one-atm tube furnaces used for the isothermal heating experiments and J. Way provided valuable assistance in locating the Tioga ash bed sample locality. Special thanks are due to W. Carlson for providing a preprint of a manuscript in press, and to B. McKay for the microprobe analyses. Critical reviews by C. Naeser, J. Corrigan, and W. Carlson and useful discussions with M. Roden, J. Watt, W. Maggs, D. Miller, E. Watson, K. Crowley, S. Willett, M. Burke, and I. Duddy and a review by P. Green of an earlier manuscript helped in many ways to formulate the ideas presented here.

References cited

Albrecht, D., Armbruster, P., Spohr, R., Roth, M., Schaupert, K., and Stuhrmann, H. (1985) Investigation of heavy ion produced defect structures in insulators by small angle scattering. Applied Physics, A37, 37–46.

Beyer, W.H. (1987) CRC standard mathematical tables (28th edition), 674 p. CRC Press, Boca Raton.

Bhandari, N., Bhat, S.G., Lal, D., Rajagopalan, G., Tamhane, A.S., and Venkatavaradan, V.S. (1971) Fission fragment tracks in apatite: recordable track lengths. Earth and Planetary Science Letters, 13, 191–199.

Carlson, W.D. (1990) Mechanisms and kinetics of apatite fission-track annealing. American Mineralogist, 75, 1120–1139.

Corrigan, J.D., and Wilson, C. (1989) Estimates of temperature versus time from apatite fission-track data. Eos, 70, 1380.

Dakowski, M. (1978) Length distributions of fission tracks in thick crystals. Nuclear Track Detection, 2, 181–189.

Dartyge, E., Duraud, J.P., Langevin, Y., and Maurette, M. (1981) New model of nuclear particle tracks in dielectric minerals. Physics Review, B23, 5213–5229.

Donelick, R.A. (1988) Etchable fission track length reduction in apatite: Experimental observations, theory and geological applications, 414 p. Unpublished Ph.D. thesis, Rensselaer Polytechnic Institute, Troy, New York.

Donelick, R.A., and Willett, S.D. (1989) Inverse modeling of apatite fission track length spectra and age to estimate temperature history. Eos, 70, 1320.

Donelick, R.A., Roden, M.K., Mooers, J.D., Carpenter, B.S., and Miller, D.S. (1990) Etchable length reduction of induced fission tracks in apatite at room temperature (23 °C): Crystallographic effects and "initial" mean lengths. Nuclear Tracks, 17, 261–265.

Dumitru, T.A. (1989) Constraints on the uplift of the Franciscan subduction complex from apatite fission track analysis. Tectonics, 8, 197–220.

Fleischer, R.L., Price, P.B., and Walker, R.M. (1964) Track registration in various solid-state nuclear track detectors. Physics Review, 133, A1443–A1449.

——— (1965) Effects of temperature, pressure, and ionization of the formation and stability of fission tracks in minerals and glasses. Journal of Geophysical Research, 70, 1497–1502.

Galbraith, R.F., and Laslett, G.M. (1988) Some calculations relevant to thermal annealing of fission tracks in apatite. Proceedings of the Royal Society of London, A419, 305–321.

Gleadow, A.J.W., and Duddy, I.R. (1981) A natural long-term track annealing experiment for apatite. Nuclear Tracks, 5, 169–174.

Green, P.F. (1981) "Track-in-track" length measurements in annealed apatites. Nuclear Tracks, 5, 121–128.

Green, P.F., and Durrani, S.A. (1977) Annealing studies of tracks in crystals. Nuclear Track Detection, 1, 33–39.

Green, P.F., Duddy, I.R., Gleadow, A.J.W., Laslett, G.M., and Tingate, P.R. (1986) Thermal annealing of fission tracks in apatite 1. A qualitative description. Chemical Geology, Isotope Geoscience Section, 59, 237–253.

Green, P.F., Duddy, I.R., Laslett, G.M., Hegarty, K.A., Gleadow, A.J.W., and Lovering, J.F. (1989) Thermal annealing of fission tracks in apatite. 4. Quantitative modelling techniques and extension to geological timescales. Chemical Geology, Isotope Geoscience Section, 79, 155–182.

Kelley, S.A., and Duncan, I.J. (1986) Late Cretaceous to middle Tertiary tectonic history of the northern Rio Grande rift. Journal of Geophysical Research, 91, 6246–6262.

Laslett, G.M., Kendall, W.S., Gleadow, A.J.W., and Duddy, I.R. (1982) Bias in measurement of fission-track length distributions. Nuclear Tracks, 6, 79–85.

Naeser, C.W. (1979) Thermal history of sedimentary basins: Fission track dating of subsurface rocks. Society of Economic Paleontologists and Mineralogists Special Publication 26, 109–112.

Naeser, C.W., and Faul, H. (1969) Fission track annealing in apatite and sphene. Journal of Geophysical Research, 74, 705–710.

Press, W.H., Flannery, B.P., Teukolsky, S.A., and Vetterling, W.T. (1986) Numerical recipes, 818 p. Cambridge University Press, Cambridge, England.

Ravenhurst, C., Donelick, R.A., and Roden, M.K. (1989) Crystallographic orientation dependence of fission track annealing kinetics in apatite. Eos, 70, 1398.

Roden, M.K., Parrish, R.R., and Miller, D.S. (1990) An absolute age of the Eifelian Tioga ash bed, Pennsylvania. Geology, 98, 282–285.

Singh, S., Singh, D., Sandhu, A.S., Singh, G., and Virk, H.S. (1986) A study of track etch anisotropy in apatite. Nuclear Tracks, 12, 927–930.

Wagner, G.A. (1981) Fission-track ages and their geological interpretation. Nuclear Tracks, 5, 15–25.

Wagner, G.A., Reimer, G.M., and Jager, E. (1977) The cooling ages derived by apatite fission track, mica Rb-Sr, and K-Ar dating: The uplift and cooling history of the Central Alps. Memoir of the Institute of Geology and Mineralogy, University of Padua, Padua, Italy, 30, 27 p.

Way, J.H., Smith, R.C., and Roden, M. (1986) Detailed correlations across 175 miles of Valley and Ridge of Pennsylvania using 7 ash beds in the Tioga zone. Pennsylvania Topographic and Geological Survey Guidebook, 51st Annual Field Conference of Pennsylvania Geologists, 55–72.

Zeitler, P.K. (1983) Uplift and cooling history of the NW Himalaya, northern Pakistan; evidence from fission track and $^{40}Ar/^{39}Ar$ cooling ages, 297 p. Ph.D. thesis, Dartmouth College, Hanover, New Hampshire.

Manuscript received March 2, 1990
Manuscript accepted November 9, 1990

Appendix 1. Notation

t duration of an individual isothermal partial annealing experiment (s)

T temperature of an individual isothermal partial annealing experiment (°C)

N number of fission tracks measured for an individual partial annealing experiment (dimensionless)

l_i measured length of fission track i (μm)

θ_i measured angle to the crystallographic c-axis of fission track i (degrees)

l_{θ_i} radius of ellipse (mean track length) at an angle θ_i to the c axis (μm)

σ_{θ_i} standard deviation of the track lengths about the radius of an ellipse at θ_i degrees to the crystallographic c-axis (μm)

θ_m arithmetic mean track angle to the crystallographic c-axis (degrees)

l_m arithmetic (conventional) mean fission track length (μm)

l_c mean fission track length parallel to the crystallographic c-axis (μm)

l_a mean fission track length perpendicular to the crystallographic c-axis (μm)

σ_m standard deviation of the track-length distribution about the arithmetic (conventional) mean (μm)

σ_e standard deviation of the track-length distribution about the ellipse (μm)

χ^2 chi-square statistic (dimensionless)

ν number of degrees of freedom (dimensionless)

Q probability of greater chi-square (dimensionless)

n empirical latent (unetched) fission track defect density distribution constant (dimensionless; Carlson, 1990)

E_a empirical activation energy constant for latent (unetched) fission track defect elimination (kJ mol^{-1}; after Carlson, 1990)

A empirical rate constant for fission track etchable length reduction (μm; Carlson, 1990)